Machining Science and Technology

ISSN: 1091-0344 (Print) 1532-2483 (Online) Journal homepage: http://www.tandfonline.com/loi/lmst20

ROTATING TOOL POINT FREQUENCY RESPONSE PREDICTION USING RCSA

C.-H. Cheng , Tony L. Schmitz & G. Scott Duncan

To cite this article: C.-H. Cheng , Tony L. Schmitz & G. Scott Duncan (2007) ROTATING TOOL POINT FREQUENCY RESPONSE PREDICTION USING RCSA, Machining Science and Technology, 11:3, 433-446

To link to this article: http://dx.doi.org/10.1080/10910340701539866

Published online: 02 Oct 2007.

Machining Science and Technology, 11:433–446

ISSN: 1091-0344 print/1532-2483 online
DOI: 10.1080/10910340701539866

Taylor & Francis
Taylor & Francis Group

ROTATING TOOL POINT FREQUENCY RESPONSE PREDICTION USING RCSA

C.-H. Cheng and Tony L. Schmitz □ *Department of Mechanical and Aerospace Engineering, University of Florida, Gainesville, Florida, USA*

G. Scott Duncan □ *Department of Mechanical Engineering, Valparaiso University, Valparaiso, Indiana, USA*

□ *This article describes the prediction of rotating tool point frequency response functions using receptance coupling substructure analysis (RCSA). In this approach, the at-speed spindle-machine dynamics are identified by impact tests of a rotating cylindrical standard artifact. After removing the portion of the artifact beyond the holder flange in simulation, models of arbitrary tool-holder combinations are coupled to the spindle response to predict the speed-dependent tool point frequency response. Given this information, process dynamics predictions for spindles that exhibit dynamic changes with rotating speed are made possible without detailed knowledge of the spindle geometry, assembly tolerances, etc. Experimental results and comparisons with prediction are provided.*

Keywords Dynamic, Milling, Receptance, Spindle, Stability, Variance

INTRODUCTION

In order to realize high productivity in milling operations, it is necessary to specify operating parameters that avoid: prohibitive tool wear, unacceptable surface location error (i.e., part geometry error caused by forced vibrations), and chatter. For the latter two limitations, models have been developed to predict process performance, which rely on accurate knowledge of the tool-holder-spindle-machine assembly frequency response function, or FRF, as reflected at the free end of the cutting tool (i.e., the tool point). See reviews in Altintas and Weck (2004) and Smith and Tlusty (1991), for example.

To determine the tool point FRF, impact testing is commonly applied. In this procedure, an instrumented hammer is used to excite the tool via an impulse and the response is measured using an appropriate transducer

Address correspondence to T. L. Schmitz, University of Florida, 237 MAE-B, Gainesville, FL 32611, USA. E-mail: moriwaki@kobe-u.ac.jp

(e.g., a low mass accelerometer), Ewins (2000). For fluted tools, however, the tool point response can only be obtained by impact testing under non-rotating conditions. In general, non-rotating measurements provide acceptable data and reliable predictions of stability and surface location error, for example, are possible. However, for some spindles, the response varies with spindle speed. This is exhibited through both natural frequency shifts and damping variations. In these cases, predictions based on the non-rotating FRF may not be sufficient (Tian and Hutton, 2001; Xiong et al., 2003; Schmitz et al., 2004; Movahhedy and Mosaddegh, 2006).

This issue has previously been addressed by developing finite element models of spindles that incorporate gyroscopic effects, centrifugal forces, and sophisticated bearing models (Jones, 1960; Shin, 1992; Chen et al., 1994a, 1994b; Jorgenson and Shin, 1998; Harris, 2001; Cao and Altintas, 2004; Altintas and Cao, 2005). However, if details of the spindle geometry, assembly tolerances, drawbar force, bearing preload, and bearing behavior are unknown (or proprietary), model development is impaired. Additionally, the damping characteristics are generally not known at the design stage and must be determined by experiment. As an alternative, we have adapted receptance coupling substructure analysis (RCSA) to handle spindles with speed-dependent dynamics (Schmitz and Duncan, 2006; Schmitz and Duncan, 2005; Schmitz et al., 2001a, 2001b; Schmitz and Donaldson, 2000).

In the RCSA approach, which is based on early work by Bishop and Johnson (1960) and more recent work by Ewins (1986) and Ferreira and Ewins (1996), a measurement of the spindle is coupled to models of arbitrary tool-holder combinations to predict the assembly response. Because the spindle dynamics are identified using a cylindrical (non-fluted) standard artifact, the method is well-suited to rotating spindle measurements. Using rotating spindle data collected at discrete intervals over the speed range of interest, at-speed tool point predictions of fluted cutters is made possible.

In the following sections we describe the steps required to complete RCSA rotating FRF predictions and provide experimental validation for the approach. The paper is organized as follows: first, a brief review of the 3-component RCSA method is provided; second, the rotating standard artifact measurement procedure is described; third, rotating FRF measurements of carbide tool blanks clamped in a high-speed spindle are compared to predictions; and finally, stability predictions based on non-rotating and rotating FRFs are compared to cutting test results using a new stability metric.

RCSA Description

Here we provide a description of the 3-component RCSA model (Schmitz and Duncan, 2005). The RCSA method is composed of

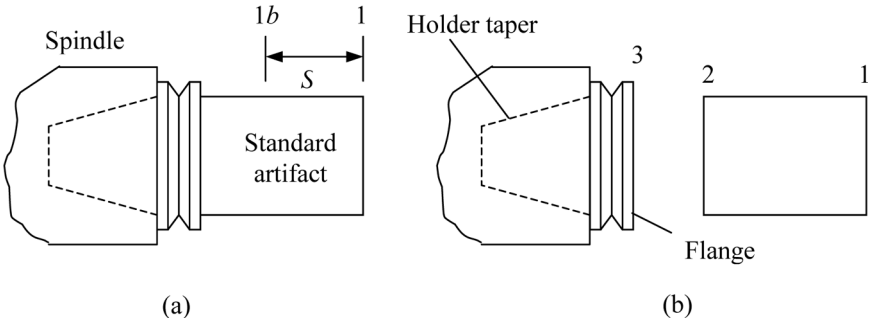

FIGURE 1 Standard artifact measurement (a) and decomposition (b).

4 fundamental steps: (1) a cylindrical standard artifact is inserted in the spindle and direct and cross FRFs[1] are recorded by impact testing; (2) the portion of the standard artifact beyond the flange is removed in simulation (i.e., inverse RCSA or decomposition) to isolate the spindle-machine response; (3) a model of the desired tool-holder is developed; and (4) the model FRF is coupled to the spindle-machine FRF.

The standard artifact measurements are depicted in Figure 1. The impulsive force is applied at locations 1 and 1*b* and the corresponding lateral translation (which may be recorded as displacement, velocity, or acceleration, depending on the selected transducer) is measured at coordinate 1. These direct and cross-translational receptances, $H_{11}(\omega) = X_1/F_1$ and $H_{11b}(\omega) = X_1/F_{1b}$ (ω is frequency), are used to synthesize the rotational receptances for the free end of the artifact-spindle-machine assembly as shown in equations (1–2), Sattinger (23), where X indicates displacement, Θ represents rotation, F indicates a harmonic force, M denotes a harmonic moment, and S is the distance between the 1 and 1*b* coordinates. The subscripts define the coordinate of interest. These artifact-spindle-machine receptances can be organized into matrix form as shown in equation (3). For these direct and cross-translational receptances, important considerations include: (1) performing the measurements far enough apart (distance S) to obtain amplitude differences that are larger than the inherent measurement noise; and (2) averaging sufficiently to reduce the noise in each measurement.

$$N_{11} = \frac{\Theta_1}{F_1} = \frac{H_{11} - H_{11b}}{S} = L_{11} = \frac{X_1}{M_1} \tag{1}$$

[1]Frequency response functions are also referred to as receptances. A direct receptance is obtained when the excitation and measurement locations coincide. A cross-receptance is obtained when they do not.

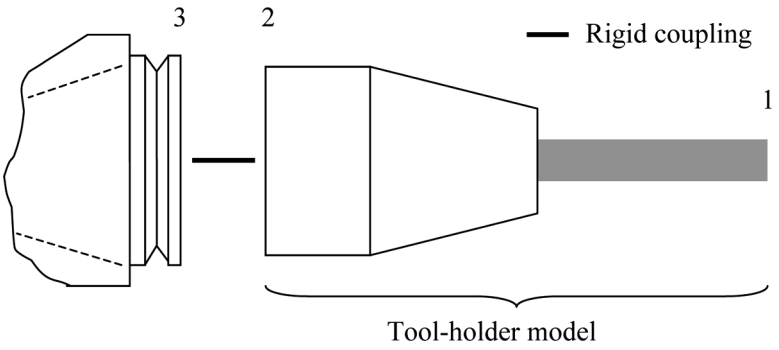

FIGURE 2 Three-component RCSA model–coordinate definitions.

$$P_{11} = \frac{\Theta_1}{M_1} = \frac{F_1}{X_1}\frac{X_1}{M_1}\frac{\Theta_1}{F_1} = \frac{L_{11}N_{11}}{H_{11}} = \frac{N_{11}^2}{H_{11}} \tag{2}$$

$$\widehat{G}_{11} = \begin{bmatrix} H_{11} & L_{11} \\ N_{11} & P_{11} \end{bmatrix} \tag{3}$$

The portion of the standard artifact beyond the flange is then removed by inverse RCSA using equation (4). Here, $G_{33} = \begin{bmatrix} h_{33} & l_{33} \\ n_{33} & p_{33} \end{bmatrix}$ is the matrix of spindle-machine receptances (including the flange and holder taper) and G_{11}, G_{12}, G_{21}, and G_{22} are the receptances derived from the beam model (e.g., Euler-Bernoulli, Bishop and Johnson (1960), or Timoshenko, Weaver et al. (1990)) for the artifact section beyond the flange. The lower case format for the *h*, *l*, *n*, and *p* terms indicates component, rather than assembly, receptances. Arbitrary models of tool-holder combinations can then be coupled to *G*33 to predict the tool point translational response, H_{11}, using equation (5). In this case, the G_{11}, G_{12}, G_{21}, and G_{22} matrices contain receptances for the tool-holder model. See Figure 2 for coordinate definitions.

$$G_{33} = G_{21}(G_{11} - \widehat{G}_{11})^{-1}G_{12} - G_{22} \tag{4}$$

$$\begin{bmatrix} H_{11} & L_{11} \\ N_{11} & P_{11} \end{bmatrix} = G_{11} - G_{12}(G_{22} + G_{33})^{-1}G_{21} \tag{5}$$

Rotating Artifact Measurements

To capture potential changes in the spindle dynamics at different rotating speeds, the standard artifact measurement sequence shown in Figure 1a is performed at a number of spindle speeds. This requires the

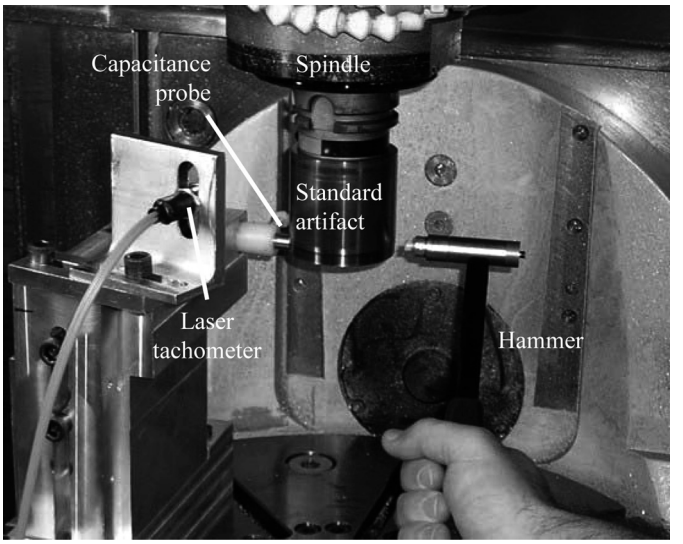

FIGURE 3 Standard artifact rotating frequency response measurement test setup. A capacitance probe is used to record the response from the instrumented hammer impulse. The laser tachometer provides a once-per-revolution signal used for subsequent data analysis.

use of a non-contact sensor to record the response from the hammer impact; we have used a capacitance probe (see Figure 3 for the test setup), but other sensors may also be applied. In any case, synchronous content in the time-domain vibration signal (due to the artifact shape with respect to the axis of rotation and axis error motions) reduces the signal-to-noise ratio (SNR) and corrupts the FRF (i.e., spurious peaks are seen at the synchronous frequencies and their harmonics). Therefore, we have implemented a time-domain filtering algorithm where a single revolution of the signal which follows the transient response from the impact excitation is collected and subtracted from the entire vibration signal.

A laser tachometer is used to identify this single revolution of post-transient data and produce multiple copies of the data. This trace is then subtracted from the original signal to remove the synchronous content. An example of this filtering procedure is provided in Figure 4. After this time-domain filtering of the vibration data, the force and vibration signals are then converted to the frequency-domain using the discrete Fourier transform and their complex ratio is calculated to obtain the FRF. This procedure is repeated many times and the FRFs are averaged to further improve SNR (we typically used 100 averages per measurement).

Another practical issue is the difficulty in impacting a rotating target. We performed several tests with variations in the hammer tip type (nylon and brass) and target surface finish (as-turned and polished) and observed no appreciable change in the measured FRF. Figure 5 displays H_{11}

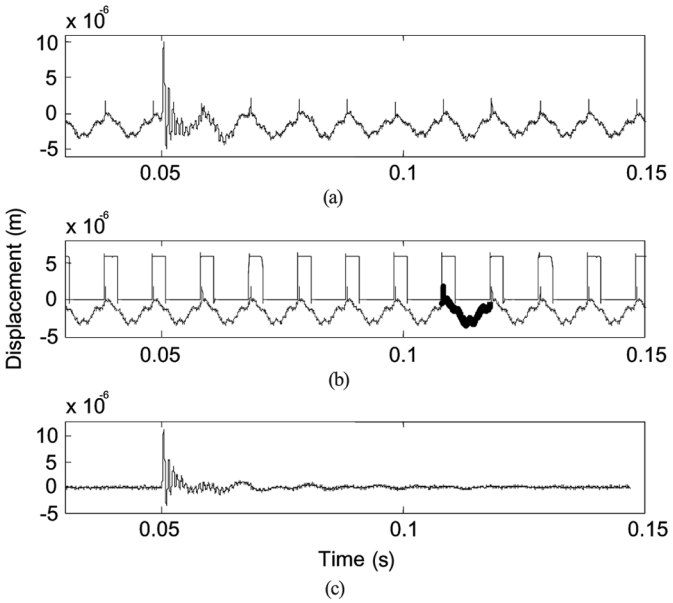

FIGURE 4 Time-domain filtering example. (a) Original capacitance probe signal with synchronous noise superimposed on response to hammer impact (applied at 0.05 s). (b) The single revolution, bold section of the post-impact transient data was identified using the tachometer signal (scaled for plotting purposes). This section was then copied to produce the trace (dotted line) to be subtracted from the original signal. (c) Displacement signal after filtering. Improved SNR is observed.

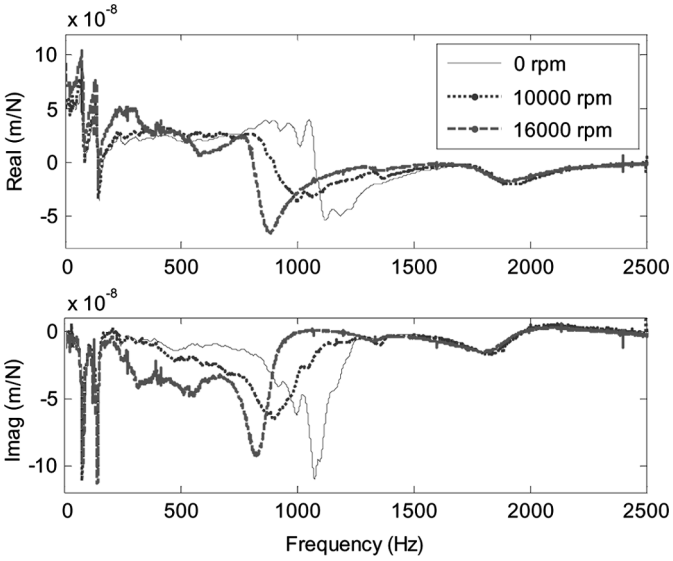

FIGURE 5 Example measurement results for rotating standard artifact (x direction). It is seen that the H_{11} measurements are spindle speed dependent. However, the spindle rigid body modes at 75 Hz and 138 Hz are consistent with rotating speed.

standard artifact measurement results at three different spindle speeds of {0, 10,000, and 16,000} rpm for the Step-Tec 20,000 rpm, 16 kW cartridge-type spindle (HSK-63A holder interface) used in this study. The spindle response clearly exhibits a dependence on spindle speed through variations in both natural frequency and amplitude. These results are for x direction measurements (according to the machine axis labeling convention). The y direction exhibited similar results. It is interesting to note that the spindle rigid body modes at 75 Hz and 138 Hz are consistent with spindle speed. This suggests that the speed-dependent response variations are probably not driven by changes in the stiffness values for the spindle bearings.

Prediction and Validation for Rotating Tool Blanks

In order to validate the RCSA approach for rotating tool FRF predictions, carbide tool blanks (no cutting edges) were used in place of fluted cutters. This enabled us not only to couple tool-holder models to spindle-machine rotating FRFs (obtained using the standard artifact), but also perform at-speed tool point frequency response measurements for comparison with predictions. Figure 6 shows the tool-holder model for a 25.4 mm diameter tool blank inserted in a collet holder. Because the Timoshenko beam element applied here, Yokoyama (1990) and Hutchinson (2001), requires a constant cross-section and material properties, the tool-holder has been divided into 5 sections. These free-free boundary condition sections are rigidly coupled to form the tool-holder model. The section dimensions and material properties are provided in Table 1, which includes the outer and inner diameters, d_{out} and d_{in}, length, L, outer and inner elastic modulus values, E_{out} and E_{in}, and outer and inner densities, ρ_{out} and ρ_{in}.

Additionally, Poisson's ratio values for steel holder and carbide tool are 0.22 and 0.29, respectively, and the structural damping coefficient is 0.0015 for both materials. The free-free tool-holder receptances determined from

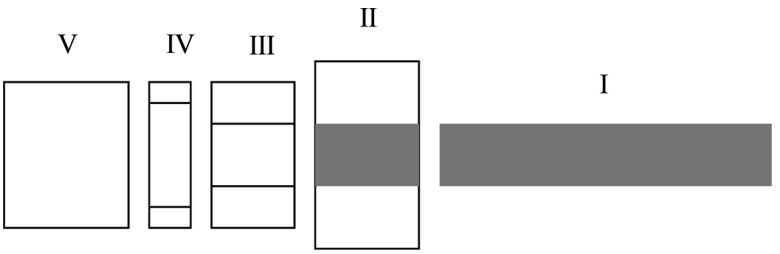

FIGURE 6 Five-section tool-holder model for 25.4 mm diameter carbide blank inserted in collet holder.

TABLE 1 Section Dimensions and Material Properties for Carbide Blank-Collet Holder

Section	d_{out} (mm)	d_{in} (mm)	L (mm)	E_{out} (N/m^2)	E_{in} (N/m^2)	ρ_{out} (kg/m^3)	ρ_{in} (kg/m^3)
I	25.4	–	127.0	5.5×10^{11}	–	14500	–
II	62.7	25.4	25.5	2×10^{11}	5.5×10^{11}	7850	14500
III	42.0	25.4	20.6	2×10^{11}	0	7850	0
IV	42.0	35.1	11.5	2×10^{11}	0	7850	0
V	42.0	–	34.0	2×10^{11}	–	7850	–

the Timoshenko model (direct and cross at each end) are coupled to the spindle-machine receptances recorded at a speed of 10,000 rpm. A comparison of the measured tool point FRF at {0 and 10,000} rpm and the predicted FRF at 10,000 rpm is shown in Figure 7. It is seen that the response at 10,000 rpm is quite different from the 0 rpm FRF and the at-speed prediction matches well with the measurement.

Stability Prediction and Validation for a Rotating Tool

As a further validation step, a tool-holder model for a 19.1 mm diameter, 4-flute, carbide endmill (76.1 mm overhang length) clamped in a shrink fit holder was developed and the predicted receptances were rigidly coupled to the spindle-machine receptances recorded at {10,000 and

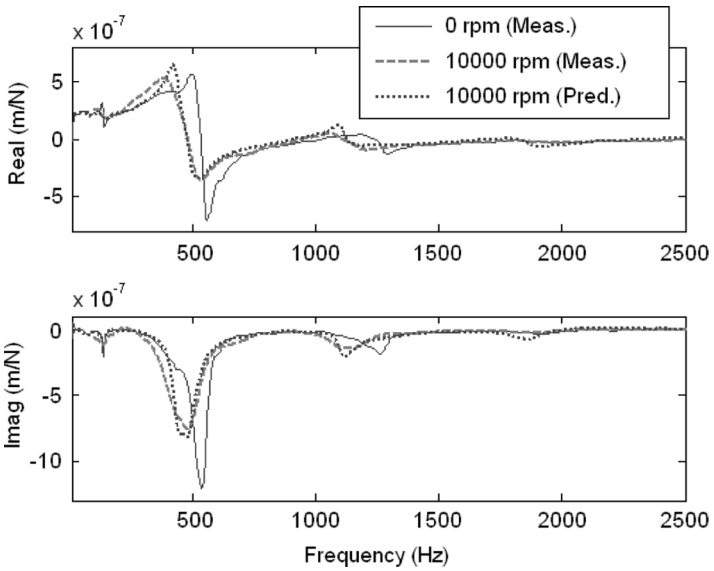

FIGURE 7 Comparison of 0 rpm measurement (solid line) to 10,000 rpm measurement (dashed) and prediction (dotted) for 25.4 mm diameter tool blank inserted in a collet holder. A significant change in the tool point FRF with speed is observed.

TABLE 2 Section Dimensions and Material Properties for Endmill-Shrink Fit Holder

Section	d_{out} (mm)	d_{in} (mm)	L (mm)	E_{out} (N/m^2)	E_{in} (N/m^2)	ρ_{out} (kg/m^3)	ρ_{in} (kg/m^3)
I	14.7	–	48.3	5.5×10^{11}	–	14500	–
II	19.1	–	27.8	5.5×10^{11}	–	14500	–
III	34.1	19.1	13.1	2×10^{11}	5.5×10^{11}	7850	14500
IV	36.2	19.1	13.1	2×10^{11}	5.5×10^{11}	7850	14500
V	38.3	19.1	13.1	2×10^{11}	0	7850	0
VI	40.4	19.1	13.1	2×10^{11}	0	7850	0
VII	41.4	19.1	10.9	2×10^{11}	0	7850	0
VIII	41.4	–	37.6	2×10^{11}	–	7850	–

16,000} rpm. The tool-holder model section dimensions and material properties are given in Table 2[2]. Stability lobes for 100% radial immersion (i.e., slotting) conditions computed from the 0 rpm and {10,000 and 16,000} rpm FRFs are shown in Figure 8, Altintas and Budak (1995). The tangential and radial cutting force coefficients for the tool/6061-T6 workpiece material combination, $k_t = 527\,\mathrm{N/mm^2}$ and $k_r = -33\,\mathrm{N/mm^2}$, respectively, were determined from separate dynamometer cutting tests as described in Altintas (2000). Significant disagreement between the stability boundaries was observed. Therefore, cutting tests were also performed to verify this behavior.

The cutting test setup is shown in Figure 9; it includes capacitance probes to measure the tool shank deflections in the x (feed) and y (perpendicular to feed in the plane of the cut) directions during cutting and a laser tachometer to enable once-per-revolution data sampling. Figure 10 shows example cutting test results, where we have defined stability using both the Fourier transform approach, Delio et al. (1992), where the sound signal is sampled and the spectral content analyzed for frequencies which do not correspond to the spindle rotating frequency or harmonics to identify chatter, and a new variance ratio, R, technique. In this method, the x and y displacements are sampled once-per-revolution to identify synchronous (stable) and asynchronous (unstable) behavior as described in Schmitz (2003).

The statistical variance in the once-per-revolution data is normalized by the variance in the overall shank motions to obtain R as shown in equation (6), where σ^2 indicates statistical variance, the x and y subscripts refer to the x and y directions, respectively, and the rev subscript identifies the once-per-revolution sampled data. For stable cutting, the tool deflections tend to repeat each revolution so the once-per-revolution variance values and, subsequently, the R value are small. For unstable cutting, on the

[2]The outer diameter for section I accounts for the reduced second area moment of inertia due to the fluted portion of the endmill, Duncan (2006).

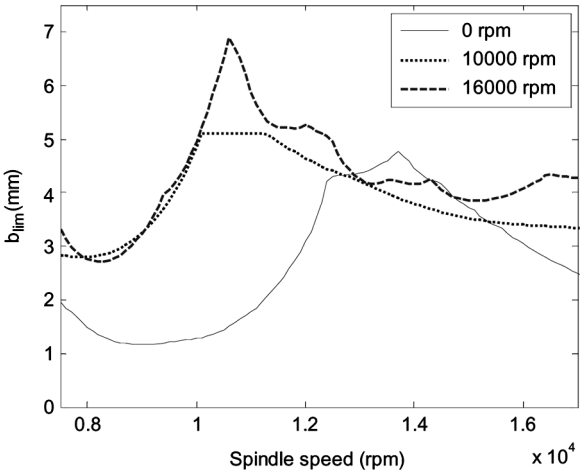

FIGURE 8 Comparison of stability boundaries for FRF measurement at 0 rpm and predictions at {10,000 and 16,000} rpm (19.1 mm diameter, four flute, carbide endmill clamped in a shrink fit holder).

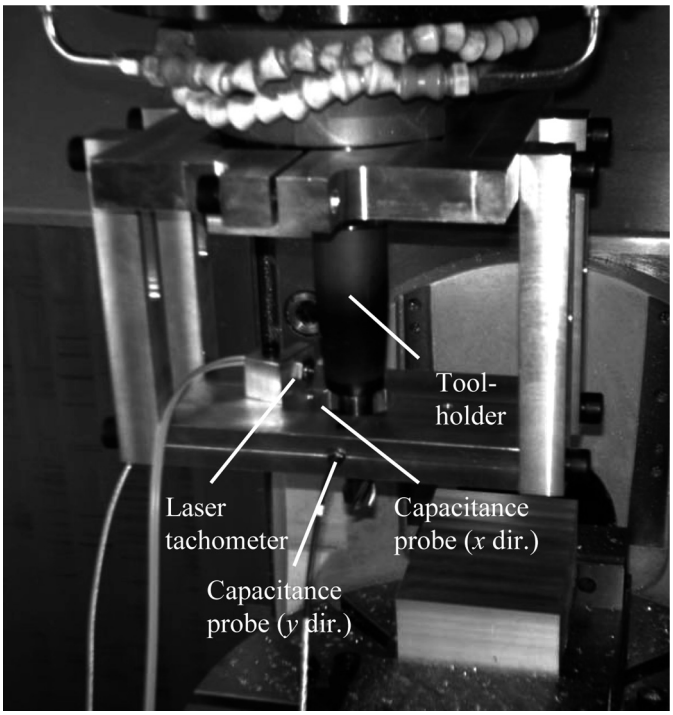

FIGURE 9 Setup for cutting tests. The tool shank deflections were measured using two orthogonal capacitance probes. A laser tachometer was used to obtain the once-per-revolution signal.

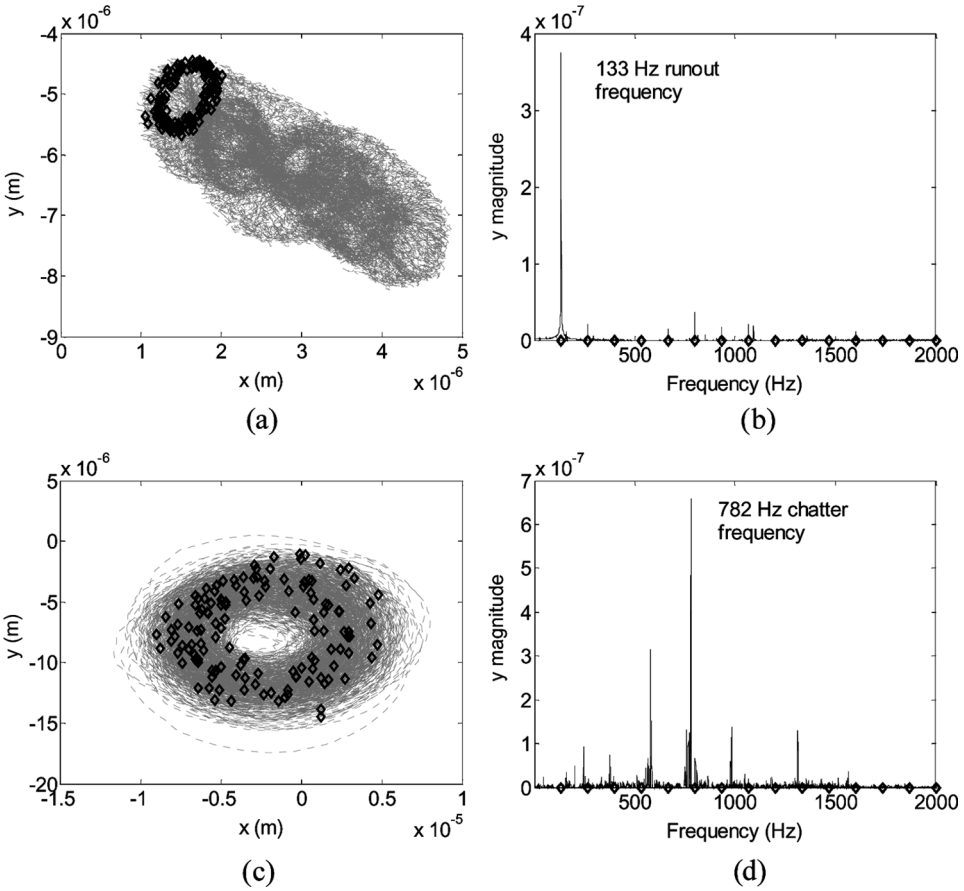

FIGURE 10 Results for 8000 rpm slotting cuts. (a) 2 mm axial depth, x vs. y displacements with once-per-revolution samples–stable with $R = 0.16$. (b) 2 mm, spectrum of y magnitude (arbitrary units)–only synchronous content is observed (frequencies identified by diamonds). (c) 2.5 mm, x vs. y displacements with once-per-revolution samples–unstable with $R = 1.0$. (d) 2.5 mm, spectrum of y magnitude–chatter frequency is observed at 782 Hz.

other hand, high R values are obtained because the vibrations occur near the system natural frequency associated with the most flexible mode, which is generally incommensurate with the spindle rotating frequency.

$$R = \frac{\sigma_{x,rev}^2 + \sigma_{y,rev}^2}{\sigma_x^2 + \sigma_y^2} \tag{6}$$

In Figure 11, the slotting test results are superimposed on the Figure 8 stability lobes. Cuts were taken to be stable when $R \leq 0.2$, marginally stable for $0.2 < R < 0.8$, and unstable when $R \geq 0.8$. These limits agreed with the

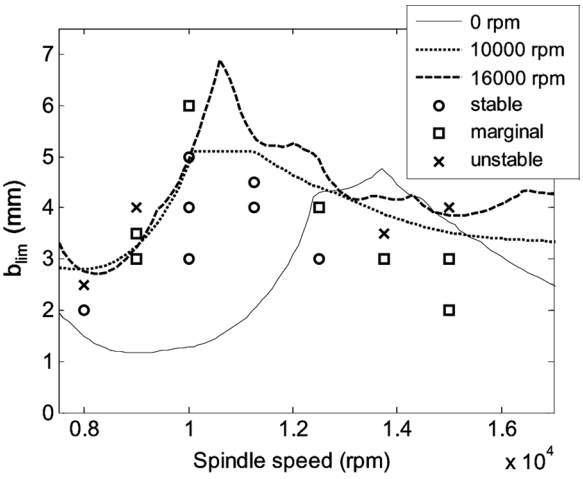

FIGURE 11 Comparison of test cut results to predicted stability boundaries determined from 0 rpm (measured) and {10,000 and 16,000} rpm (predicted) FRFs.

Fourier analysis, but additional testing will be required to determine if they can be applied to other cutting conditions. Improved agreement with experiment is seen for the stability lobes computed using the tool point FRF predictions based on the rotating standard artifact measurements. In particular, the cuts in the 10,000 rpm range exceed the boundary predicted from the 0 rpm impact test in all instances.

CONCLUSIONS

This article describes the application of receptance coupling substructure analysis (RCSA) to tool point frequency response prediction for rotating cutting tools. This capability is of particular importance when the spindle response varies with rotating speed. This approach provides an alternative to a full spindle finite element model, which requires detailed knowledge of the spindle geometry, assembly tolerances, drawbar force, bearing preload, and bearing behavior, as well as damping estimates. The method is carried out in four steps: (1) a cylindrical standard artifact is inserted in the spindle and direct- and cross-rotating frequency response functions are recorded at a finite number of spindle speeds by impact testing (non-contact vibration sensor); (2) the portion of the standard artifact beyond the flange is removed by inverse RCSA to isolate the spindle-machine response at each speed; (3) a model of the desired tool-holder is developed; and (4) the model response is coupled to the spindle-machine response at each tested speed. These rotating frequency response functions can then be used together with process models to predict

milling behavior. Good agreement between experiment and prediction for both tool point frequency response measurements and stability tests is demonstrated.

ACKNOWLEDGMENTS

The authors gratefully acknowledge support of this research by the National Science Foundation (Grant No. DMI-0238019). Any opinions, findings, and conclusions or recommendations expressed in this material are those of the authors and do not necessarily reflect the views of this agency.

REFERENCES

Altintas, Y. (2000) *Manufacturing Automation*, Cambridge University Press, Cambridge, UK.

Altintas, Y.; Budak, E. (1995) Analytical prediction of stability lobes in milling. *Annals of the CIRP*, 44(1): 357–362.

Altintas, Y.; Cao, Y. (2005) Virtual design and optimization of machine tool spindles. *Annals of the CIRP*, 54(1): 379–382.

Altintas, Y.; Weck, M. (2004) Chatter stability of metal cutting and grinding. *Annals of the CIRP*, 53(2): 629–642.

Bishop, R.E.D.; Johnson, D.C. (1960) *The Mechanics of Vibration*, Cambridge University Press, Cambridge, UK.

Cao, Y.; Altintas, Y. (2004) A general method for the modeling of spindle-bearing systems. *Journal of Mechanical Design*, 126(6): 1089–1104.

Chen, C.; Wang, K.; Shin, Y. (1994a) An integrated approach toward the dynamic analysis of high-speed spindles, Part 1: System model. *Journal of Vibrations and Acoustics*, 116: 506–513.

Chen, C.; Wang, K.; Shin, Y. (1994b) An integrated approach toward the dynamic analysis of high-speed spindles, Part 2: Dynamics under moving end load. *Journal of Vibrations and Acoustics*, 116: 514–522.

Delio, T.; Tlusty, J.; Smith, S. (1992) Use of audio signals for chatter detection and control. *Journal of Engineering for Industry*, 114: 146–157.

Duncan, G.S. (2006) Milling dynamics prediction and uncertainty analysis using receptance coupling substructure analysis, Ph.D. Dissertation, University of Florida, Gainesville, FL <http://highspeed-machining.mae.ufl.edu/htmlsite/duncan_g.pdf>.

Ewins, D.J. (1986) Analysis of modified or coupled structures using FRF properties. Internal Report 86002, Dynamics Section, Department of Mechanical Engineering, Imperial College, London, UK.

Ewins, D.J. (2000) *Modal Testing: Theory, Practice and Application*, Research Studies Press, Ltd., Philadelphia, PA.

Ferreira, J.V.; Ewins, D.J. (1996) Nonlinear receptance coupling approach based on describing functions. In *Proceedings of the 14th International Modal Analysis Conference*, Dearborn, MI, pp. 1034–1040.

Harris, T. (2001) *Rolling Bearing Analysis*, 4th edition, John Wiley & Sons, New York.

Hutchinson, J. (2001) Shear coefficients for timoshenko beam theory. *Journal of Applied Mechanics*, 68: 87–92.

Jones, A. (1960) A general theory for elastically constrained ball and radial roller bearings under arbitrary load and speed conditions. *Journal of Basic Engineering*, 82: 309–320.

Jorgenson, B.; Shin, Y. (1998) Dynamics of spindle-bearing systems at high speeds including cutting load effects. *Journal of Manufacturing Science and Engineering*, 120: 387–394.

Movahhedy, M.R.; Mosaddegh, P. (2006) Prediction of chatter in high speed milling including gyroscopic effects. *International Journal of Machine Tools & Manufacture*, 46(9): 996–1001.

Sattinger, S. (1980) A method for experimentally determining rotational mobilities of structures. *Shock and Vibration Bulletin*, 50: 17–27.

Schmitz, T. (2003) Chatter recognition by a statistical evaluation of the synchronously sampled audio signal. *Journal of Sound and Vibration*, 262(3): 721–730.

Schmitz, T.; Davies, M.; Kennedy, M. (2001a) Tool point frequency response prediction for high-speed machining by RCSA. *Journal of Manufacturing Science and Engineering*, 123: 700–707.

Schmitz, T.; Davies, M.; Medicus, K.; Snyder, J. (2001b) Improving high-speed machining material removal rates by rapid dynamic analysis. *Annals of the CIRP*, 50(1): 263–268.

Schmitz, T.; Donaldson, R. (2000) Predicting high-speed machining dynamics by substructure analysis. *Annals of the CIRP*, 49(1): 303–308.

Schmitz, T.; Duncan, G.S. (2006) Receptance coupling for dynamics prediction of assemblies with coincident neutral axes. *Journal of Sound and Vibration*, 289(4–5): 1045–1065.

Schmitz, T.; Duncan, G.S. (2005) Three-component receptance coupling substructure analysis for tool point dynamics prediction. *Journal of Manufacturing Science and Engineering*, 127(4): 781–790.

Schmitz, T.; Ziegert, J.; Stanislaus, C. (2004) A method for predicting chatter stability for systems with speed-dependent spindle dynamics. SME technical paper TP04PUB182, *Transactions of NAMRI/SME*, 32: 17–24.

Shin, Y. (1992) Bearing nonlinearity and stability analysis in high-speed machining. *Journal of Engineering for Industry*, 114: 23–30.

Smith, S.; Tlusty, J. (1991) An overview of modeling and simulation of the milling process. *Journal of Engineering for Industry*, 113: 169–175.

Tian, J.; Hutton, S. (2001) Chatter instability in milling systems with flexible rotating spindles—a new theoretical approach. *Journal of Manufacturing Science and Engineering*, 123: 1–9.

Weaver, Jr., W.; Timoshenko, P.; Young, D. (1990) *Vibration Problems in Engineering*, 5th edition, John Wiley & Sons, New York.

Xiong, G.L.; Yi, J.M.; Zeng, C.; Guo, H.K.; Li, L.X. (2003) Study of the gyroscopic effect of the spindle on the stability characteristics of the milling system. *Journal of Materials Processing Technology*, 138: 379–384.

Yokoyama, T. (1990) Vibrations of a hanging Timoshenko beam under gravity. *Journal of Sound and Vibration*, 141: 245–258.